The carbon dioxide signal from the COVID-19 lock-down

John Reid (johnsinclairreid@gmail.com)

Article

Keywords:

Posted Date: August 18th, 2020

DOI: https://doi.org/10.21203/rs.3.rs-57102/v1

The carbon dioxide signal from the COVID-19 lock-down

August 11, 2020

Abstract

Two unintended experiments provide insight into the role of anthropogenic emissions in the global carbon cycle. One was the temporary reduction in emissions during the COVID-19 lock-down. The other was the emission of a radioactive isotope of carbon during the testing of nuclear weapons in the 1950s and the abrupt cessation of these tests in 1963. Together they imply the existence of two distinct reservoirs which exchange carbon with the atmosphere, viz.: the mixed layer and the deep ocean. Exchanges with the former are noisy because they are influenced by sea surface temperature which, in turn, depends on local weather conditions. They completely mask any variations caused by the COVID-19 lock-down. Exchanges with the latter are steady, long-term and uninfluenced by the weather. They result in half the carbon content of the atmosphere and mixed layer being replaced every eleven years.

1 Carbon Dioxide Measurements

Before the COVID-19 pandemic of 2020, emissions of carbon dioxide were rising by about one percent per year over the previous decade. Government policies during the COVID-19 pandemic changed patterns of energy demand around the world due to reduced transport and changed consumption patterns. This short, unexpected and random variation in emissions allows bounds to be placed on the magnitude of the response of the global carbon system to this sudden fall in production rate.

The temporary reduction in in CO_2 emissions due to the lockdown have recently been described quantitatively[1]. Daily global CO_2 emissions decreased by seventeen percent by early April 2020 compared with the mean 2019 levels. At their peak, emissions in individual countries decreased by 26 percent on average. At issue is whether this perturbation was detected by any of the atmospheric baseline monitoring stations around the world. Here we look at data from two, the Cape Grim Observatory[2] in Tasmania and the Mauna Loa Observatory in Hawaii[3, 4] (Figure 1).

Let $\dot{m}$ be the rate of anthropogenic emissions of CO_2, then Figure 3b of [1] shows that the dip in $\dot{m}$, $\Delta\dot{m}$, during the first five months of 2020 to be about

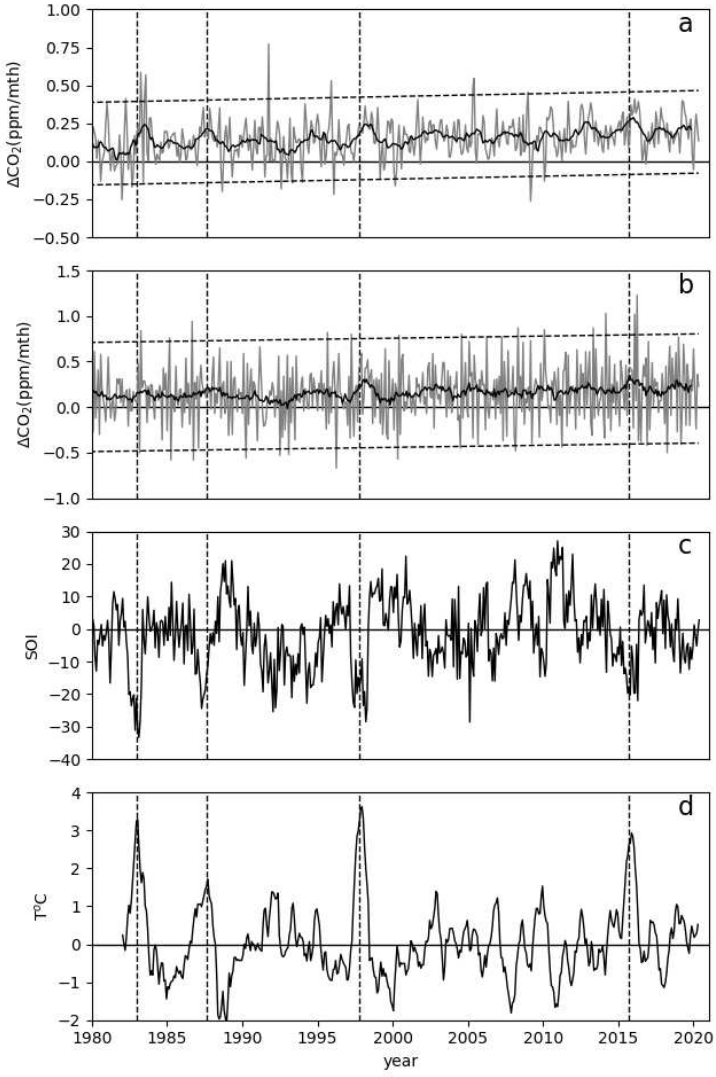

Figure 1: Monthly rate of change in atmospheric CO2 concentration (grey) and 13 month running mean (black) at Cape Grim (**a**) and Mauna Loa (**b**). Horizontal dashed lines show 2σ confidence limits. **c**. Southern Oscillation Index. **d**. Sea Surface Temperature anomaly of the Nino 3 region of the Equatorial Pacific. Vertical dashed lines are times of peak SST.

15 Mt per day, i.e $15 \times 10^{-3} \times (365/12) = .45$ Pg/month. For a well-mixed atmosphere, the corresponding dip, $\Delta\dot{c}$, in the rate of change of concentration of CO_2, c, is given by

$$\Delta\dot{c} = \frac{\Delta\dot{m}}{M} \tag{1}$$

where $M = 5.15 \times 10^6$ Pg is the mass of the atmosphere. Substituting in (1) and multiplying by 10^6 to give parts per million yields $\Delta\dot{c} = .087$ ppm/month.

Values of $\dot{c}$ derived as the first differences of the monthly average concentration, c, measured at the Cape Grim and Mauna Loa observatories are shown in Figure 1a and Figure 1b respectively. Thirteen month running means are also shown. There is a significant linear trend in both time series. The standard deviations, σ, of the residuals were 0.14 and 0.30 ppm/month respectively. The dashed lines show the 2σ confidence limits above and below the trend lines. The expected fall in $\Delta\dot{c}$ of .087 ppm/month is thus too small to be evident in the observations. On a time scale of months the COVID-19 lock-down event was masked by ongoing natural processes.

The two lower panels give an indication of what such natural processes might be. Figure 1c shows the Southern Oscillation Index for the period in question. The SOI is calculated from the sea level pressure difference between Tahiti and Darwin. Sustained negative excursions of the SOI are termed El Niño events and are associated with increases in Sea Surface Temperature in the Eastern Equatorial Pacific as shown in Figure 1d for the Niño3 region (5°N-5°S, 150°W-90°W)[5]. The times of the SST peaks in Figure 1d are shown by vertical dashed lines in all four panels.

All four El Niño warming events are associated with increases in the running means of atmospheric CO_2 concentration at both Cape Grim and Mauna Loa. This is not surprising. The solubility of CO_2 in sea water is strongly dependent on temperature and it comes out of the ocean when SST increases. In general, the high frequency noisiness of the monthly differences can be accounted for by the degassing and absorption of CO_2 by the upper part of the ocean as it is heated and cooled by changing weather systems.

2 The Bomb Test Curve

The testing of nuclear weapons during the 1950s and 1960s injected significant amounts of the radioactive ^{14}C isotope of carbon into the atmosphere. More importantly, the abrupt cessation of atmospheric testing following the Nuclear Test Ban Treaty of 5 August 1963, meant that the rate of production of the ^{14}C isotope reverted to the constant natural background level. This allows the movement of carbon dioxide between natural reservoirs to be assessed in much the same way that radioactive isotopes are used to assess the rates of metabolic processes in nuclear medicine.

The decrease in $\Delta^{14}C$ is known as "The Bomb Test Curve". Numerous observations were made in the decades following the cessation of testing following the Nuclear Test Ban Treaty. Here we look at a single high quality data set from

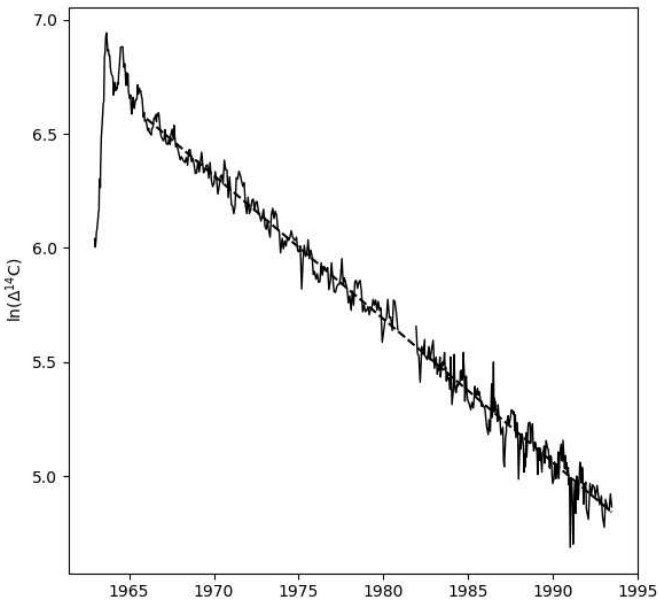

Figure 2: The natural logarithm of Δ^{14}C values recorded at Fruholmen, Norway as a function of time[6]. Dashed line: regression line fitted between January 1966 and June 1993.

.

Fruholmen, Norway[7] shown in Figure 2. The natural logarithm, $\ln(\Delta^{14}\mathrm{C})$, is plotted on the vertical axis rather than Δ^{14}C itself so that exponential behaviour becomes linear. A regression line was fitted between January 1966 and the end of the data set in June 1993.

Regression statistics are shown in Table 1. The fit is remarkably good and accounts for 98.8 percent of the variance. Hence, with a high degree of accuracy:

$$\Delta^{14}C = Ae^{-t/\tau} \tag{2}$$

where A is the value of Δ^{14}C at $t = 0$ and τ is the time constant given by $\tau = -1/\text{slope} = 15.9 \pm 0.085$ years. The time for Δ^{14}C to decay to half its initial value is given by $t_{1/2} = -\tau \ln(0.5) = 11.02 \pm .059$ years.

Thus half of the bomb test $^{14}CO_2$ disappears from the atmosphere every 11 years. Equation (2) is the solution of the classic diffusion equation:

$$\frac{dc}{dt} + \frac{c}{\tau} = F(t) \tag{3}$$

Statistic	Value
slope	-.06289
intercept	-7.76×10^{-15}
r	-0.9939
r^2	0.9878
standard error	.0003395

Table 1: Regression Statistics

where c is the concentration of the quantity being diffused ($\Delta^{14}CO_2$ in this case), τ is the diffusion time or time constant and $F(t)$ specifies the rate at which concentration increases due to new material being introduced into the reservoir. In this case following the cessation of nuclear testing $F(t)$ is the constant background rate associated with the bombardment of upper atmosphere Nitrogen by cosmic rays.

Carbon dioxide reacts with water to form carbonate and bicarbonate ions. Hence the diffusion rate of carbon *per se* involves reaction rates and diffusion rates for each of these three species. These are almost completely independent of atomic mass[8] and so all the isotopes of carbon, ^{12}C, ^{13}C, ^{14}C, in the form of CO_2 and its radicles, diffuse through water at the same rate and the time constant, τ, in (3) applies equally to all isotopic species of CO_2.

It is therefore reasonable to assume that CO_2 diffuses from the atmosphere into some other reservoir or sink. The excellent fit of a single regression line indicates that any diffusion process must be dominated by a single sink with a single time constant. Furthermore the fact that the atmospheric $\Delta^{14}CO_2$ has, by now, returned to its pre-bomb background level implies that the sink is much larger than the source, the atmosphere. The only candidate sink which fulfils these conditions is the ocean.

3 Upwelling and the Redfield ratios

Since the atmosphere has not been depleted of CO2 by this diffusion process we conclude there must be some way in which CO_2 is returned to the atmosphere. This occurs in regions of upwelling where deep ocean water outcrops into the mixed layer. There are a number of such regions in the world. They are commonly associated with western boundary currents, high levels of primary production and rich fisheries.

At decadal time scales, equation (3) can be rewritten

$$\frac{dc}{dt} + \frac{c}{\tau} = A(t) + U(t) \tag{4}$$

where τ is the diffusion time evaluated above, A(t) is the anthropogenic production rate and U(t) is the production rate from deep ocean upwellings. Here c is the concentration of CO_2 in the atmosphere and mixed layer (assumed to

Name	Symbol	Value
rate of change of concentration	dc/dt	13.9
concentration	c	2860
time constant	τ	15.9
anthropogenic production rate	$A(t)$	36.5

Table 2: Present day values of variables in equation (4) in units of $PgCO_2$/year.

be in equilibrium at these longer time scales). $U(t)$ can be evaluated in from the other terms in (4) listed in Table 2 giving $U(t) = 157$ $PgCO_2$/year.

The World Ocean Circulation Experiment (WOCE) aimed to establish the role of the World Ocean in the Earth's climate system. WOCE's field phase ran between 1990 and 1998, and was followed by an analysis and modelling phase that ran until 2002. Ganachaud and Wunsch[9] used high resolution trans-oceanic section gathered during WOCE in an inverse model to improve estimates of the global circulation and heat flux. Here we use their estimate of upwelling in just one area of the ocean together with WOCE chemical data to demonstrate the scale of this mechanism.

The area chosen was the entire Atlantic between WOCE sections A02 (45° N) and A10 (30° S). It includes two major upwellings along its eastern land boundary. According to Figure 2 of [9], the total upwelling in this box is 10 ± 2.5 Sv.

Seemingly all that is needed for a rough estimate of the rate of CO_2 upwelling is to multiply this flux of seawater with the average concentration but this would overlook the the role of phytoplankton in removing CO_2 by photosynthesis when the up-welled nutrient is illuminated by sunlight. The Redfield ratio[10] is the atomic ratio of carbon, nitrogen and phosphorus (C:N:P=106:16:1) found in marine phytoplankton. Thus in the up-welled water 106 atoms of carbon are removed for each 16 atoms of nitrogen. However the concentration of carbon in the deep Atlantic is well in excess of the Redfield ratio and it is the remaining fraction which ends up in the mixed layer and the atmosphere.

Visual examination of the WOCE Section A09 of the Atlantic[11] shows a CO_2 concentration of around 2200 μmole/kg whereas that of Nitrate is generally less than about 23 μmole/kg. Multiplying the nitrate concentration by 106/16 and subtracting leaves 2050 μmole/kg of CO_2 in the mixed layer after phytoplankton has absorbed these nutrients. Other WOCE Atlantic sections show much the same concentrations of nitrogen, carbon and hence excess carbon as does this section, so that, within, say ten percent, this value pertains to the entire Atlantic Ocean below 1500m. Multiplying by the the upwelling rate gives a rate of upwelling of 76 Mt/day of CO_2 = 28 Pg/year of CO_2 = 7.6 Pg/year of carbon. These values are of the same order as the the anthropogenic emission rates quoted in [1]. Given that this calculation included only the Atlantic Ocean, the global value of 157 Pg/year of CO_2 calculated in the previous section is not unreasonable.

4 Discussion

The precise fit of the regression line in Figure 2 is in sharp contrast to the noisiness of the monthly rates of change shown Figure 1. This apparent contradiction is resolved when we consider the mixed layer[12]. The mixed layer is a turbulent layer in which winds and waves have homogenized temperature and chemistry down to some depth which varies between about 10m and 200m. Wind stress increases the depth while solar radiation in calm conditions renews stratification. Because of its turbulent nature, the mixed layer is in intimate contact with the atmosphere, so that heat and soluble gases exchange rapidly between the two reservoirs. The highly stratified thermocline lies below the mixed layer. Apart from regions of upwelling, heat and dissolved substances are transferred through the thermocline by diffusion.

In effect then, there are three reservoirs: the atmosphere, the mixed layer and the deep ocean. At time scales of months, exchange of CO_2 between the mixed layer and the atmosphere predominate whereas at time scales of years to decades, the exchange of CO_2 between the deep ocean and the mixed layer predominates. At these longer time scales the mixed layer and atmosphere can be regarded as a single reservoir. The rapid variations in temperature seen in Figure 1**d** only involve the atmosphere and the mixed layer. On the other hand the variation in $\Delta^{14}CO_2$ of Figure 2 is the result of the much slower rate of diffusion of $^{14}CO_2$ from the atmosphere/mixed layer reservoir into the deep ocean.

Both time series of raw atmospheric concentration data from Cape Grim and Mauna Loa are dominated by the exponential upward trend caused by anthropogenic emissions as seen in ice core data[13]. As with the data of Figure 2, this trend can be removed by fitting a straight line to the logarithm of the raw values. The periodogram of the residuals which remain after removing the trend are shown in Figure 3. Figure 3**a** (grey) shows the periodogram, P, of the $\ln(c_t)$ residuals where $\{c_t\}$ is the sequence of weekly average CO_2 concentrations measured at Mauna Loa. The two peaks are the seasonal variation and its second harmonic. At low frequencies there is a power law trend with index -2, implying that the sequence is the outcome of a random walk process, or centrally biased random walk. Such behaviour implies integration with respect to time. Temperature is the integration of heat transfer according to Fourier's Heat Equation[14]. This supports the view that short term variations in atmospheric CO_2 concentrations are driven by sea surface temperature variations.

Figure 3**b** shows the periodogram of the residuals after removal of the exponential decay from the $\Delta^{14}CO_2$ data of Figure 2. The variance (the area under the spectrum) is much smaller than that of the Mauna Loa data. The spectrum is "white", i.e. flat, implying that the residuals are unselfcorrelated. This indicates that departures from the fitted curve are not systematic and can be attributed to experimental error.

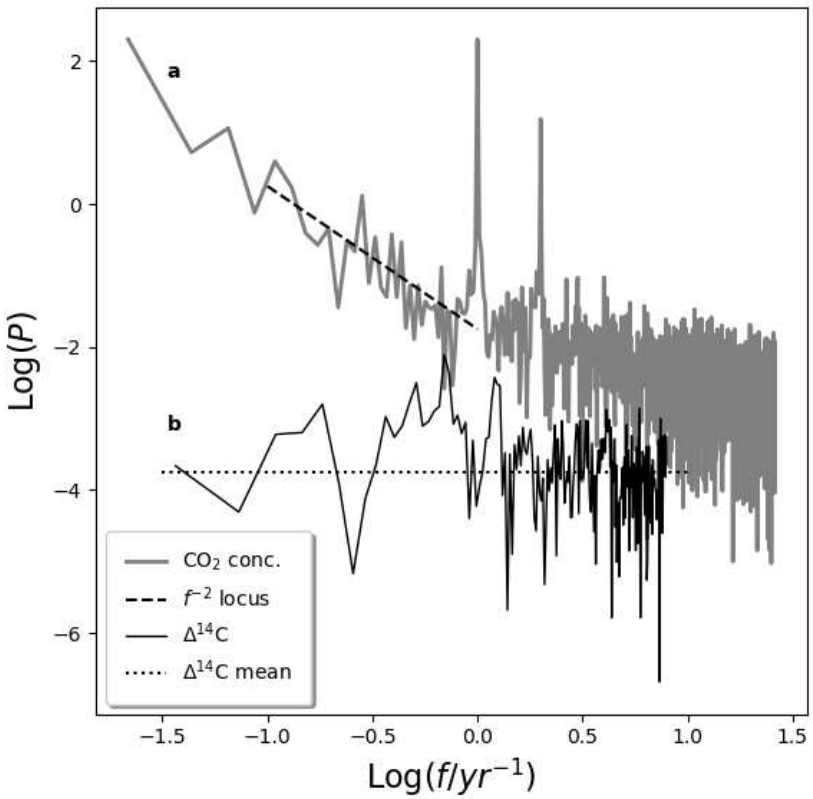

Figure 3: Variance density spectra of residuals remaining after subtracting the regression line fitted to two time series. **a** Residuals from fitting the Mauna Loa weekly average CO2. **b** Residuals from fitting the Δ^{14}C data of Figure 2. The dashed line shows the f^{-2} power law slope, indicating a random walk.

.

5 Conclusions

Month by month variations in atmospheric carbon dioxide concentrations from natural causes mask any variation from the recent COVID-19 lock-down. Such rapid variations are due to the absorption and out-gassing of CO_2 by the mixed layer of the ocean as it is warmed and cooled by fluctuating weather systems such as El Niño.

At longer time scales, the response of the carbon dioxide concentration in the atmosphere to a perturbation in production rate is governed by a first order differential equation. Hence variations over time are smoothed by the convolution of the perturbation with the impulse response curve characterised by that equation. The impulse response curve is similar to the Bomb Test Curve and has a time constant of 15.9 years. A perturbation in production rate would need to last for a comparable time in order to be detectable as a change in concentration.

References

1. Le Quéré, C. *et al.* Temporary reduction in daily CO2 emissions during the COVID-19 forced confinement. *Nat. Clim. Chang.* doi:`https://doi.org/10.1038` (2020).
2. (Accessed 24/6/2020). `https://www.csiro.au/en/Research/OandA/Areas/Assessing-our-climate/Latest-greenhouse-gas-data`.
3. Keeling, R. *et al.* in *Trends: A Compendium of Data on Global Change.* Data downloaded from https://www.esrl.noaa.gov/gmd/ccgg/trends/data.html, July 2020 (Carbon Dioxide Information Analysis Center, Oak Ridge National Laboratory, U.S. Department of Energy, Oak Ridge, Tenn., U.S.A., 2009). doi:`10.3334/CDIAC/atg.035`.
4. (Accessed 24/6/2020). `https://www.esrl.noaa.gov/gmd/ccgg/trends/data.html`.
5. Trenberth, K. E. The Definition of El Niño. *Bulletin of the American Meteorological Society* **78,** 2771–2778 (Dec. 1997).
6. (Accessed 24/6/2020). `https://cdiac.ess-dive.lbl.gov/ftp/ndp057/F.asc`.
7. Nydal, R. & Lövseth, K. Tracing bomb 14 C in the atmosphere, 1962-1980. *Journal of Geophysical Research* **88,** 3621–42 (1983).
8. Zeebe, R. E. On the molecular diffusion coefficients of dissolved CO,HCO3-, and CO32- and their dependence on isotopic mass. *Geochimica et Cosmochimica Acta* **75,** 2483–2498 (May 2011).
9. Ganachaud, A. & Wunsch, C. Improved estimates of global ocean circulation, heat transport and mixingfrom hydrographic data. *Nature* **408,** 453–457 (2000).

10. Redfield, A. On the proportions of organic derivatives in sea water and their relation to the composition of plankton. *James Johnstone Memorial Volume* **176.** Downloaded 19/7/2020, 176–192 (1934).

11. (Accessed 24/6/2020). `http://whp-atlas.ucsd.edu/whp_atlas/atlantic/a09/sections/printatlas/A09_TCARBN.jpg`.

12. Kraus, E. & Turner, J. A one-dimensional model of the seasonal thermocline II. The general theory and its consequences. *Tellus* **19,** 98–106 (1967).

13. Etheridge, D. M. *et al.* Natural and anthropogenic changes in atmospheric CO2 over the last 1000 years from air in Antarctic ice and firn. *J. Geophys. Res.* **101,** 4115–4128 (1996).

14. Hasselmann, K. Stochastic climate models, Part I, Theory. *Tellus* **XXVIII,** 473–485 (1976).

Figures

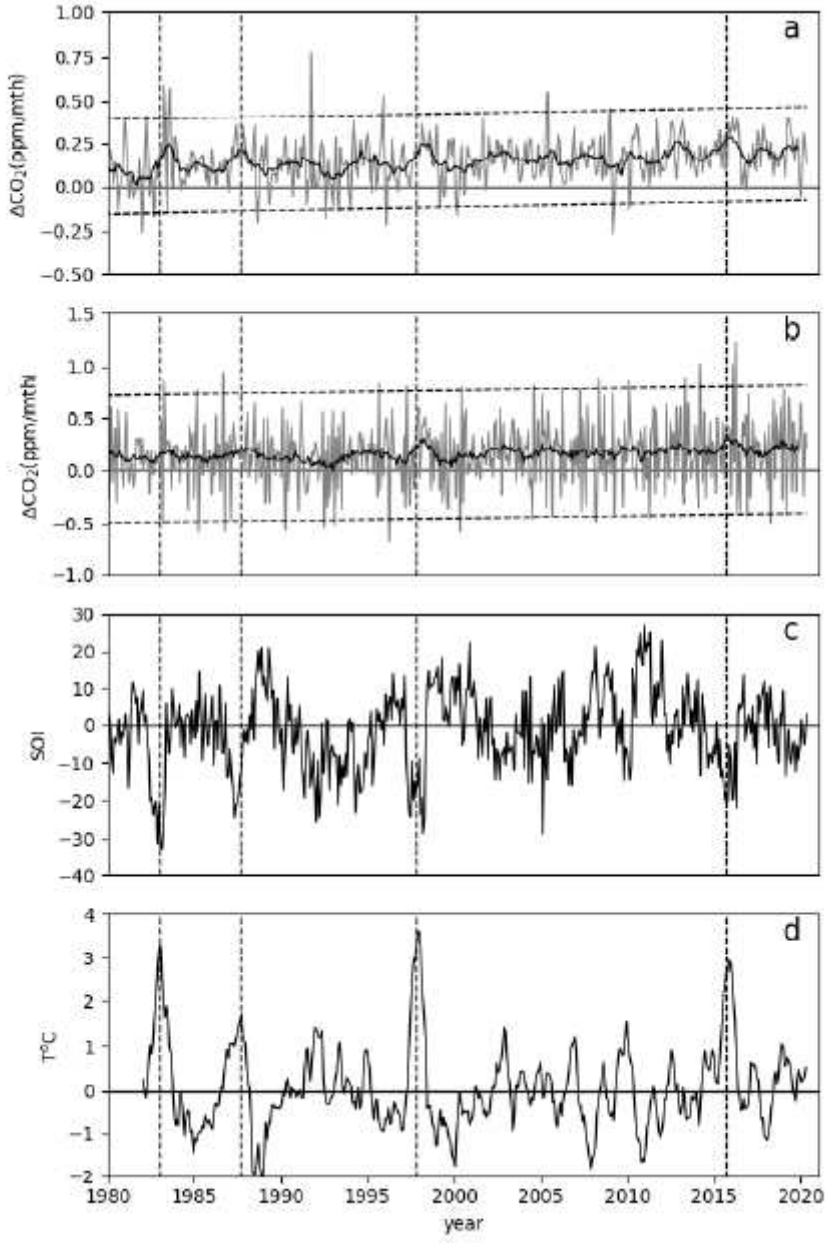

Figure 1

Monthly rate of change in atmospheric CO2 concentration (grey) and 13 month running mean (black) at Cape Grim (a) and Mauna Loa (b). Horizontal dashed lines show 2 condence limits. c. Southern Oscillation Index. d. Sea Surface Temperature anomaly of the Nino 3 region of the Equatorial Pacic. Vertical dashed lines are times of peak SST.

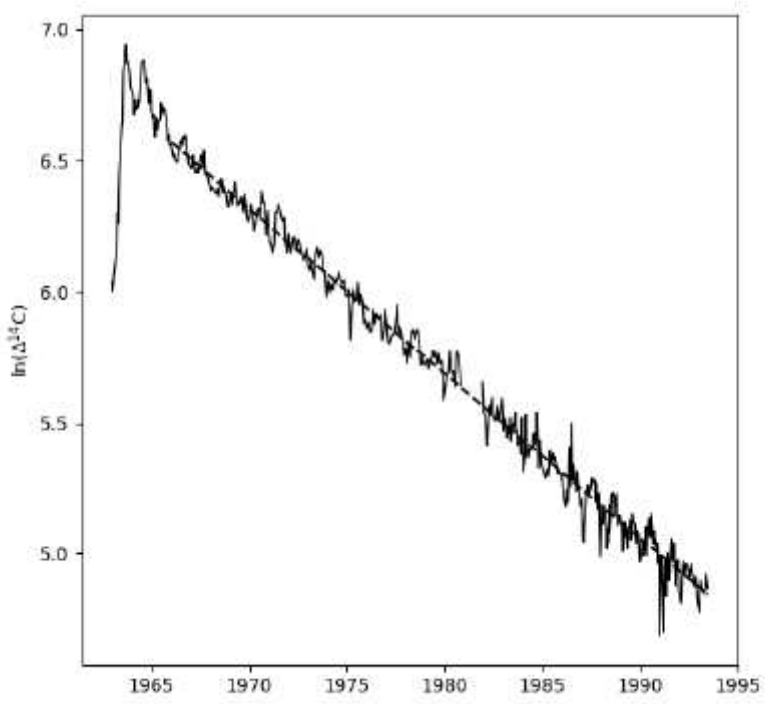

Figure 2

The natural logarithm of 14C values recorded at Fruholmen, Norway as a function of time[6]. Dashed line: regression line tted between January 1966 and June 1993.

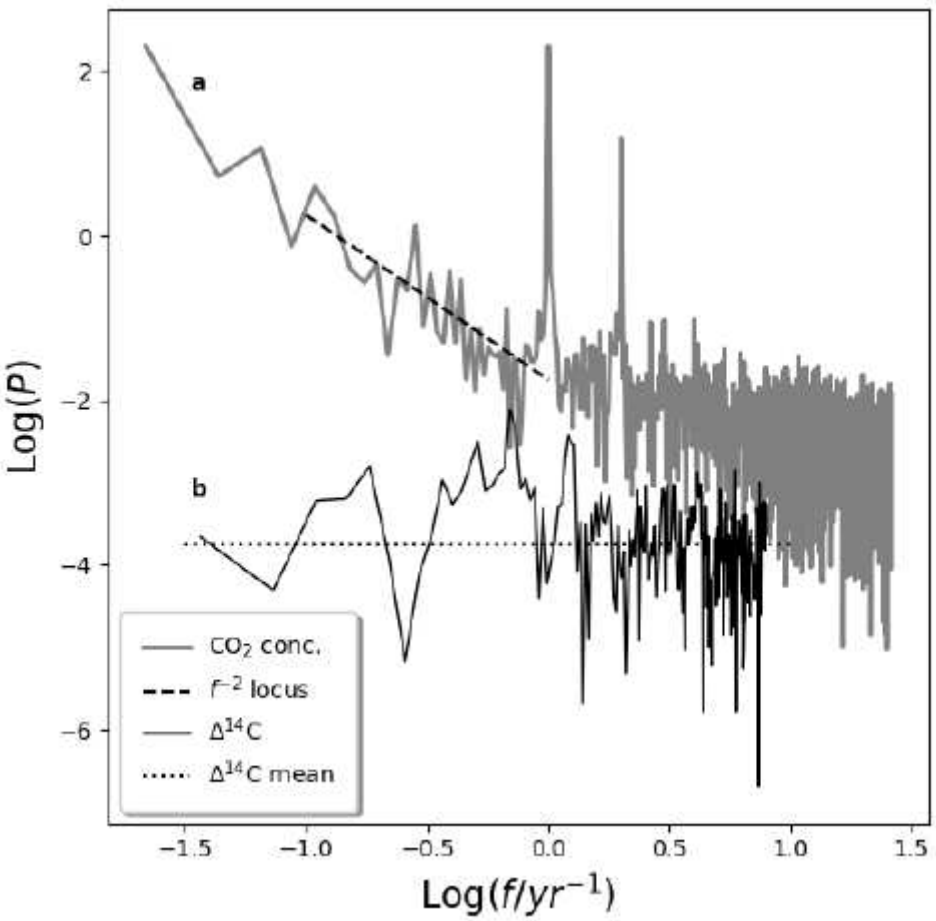

Figure 3

Variance density spectra of residuals remaining after subtracting the regression line tted to two time series. a Residuals from tting the Mauna Loa weekly average CO2. b Residuals from tting the 14C data of Figure 2. The dashed line shows the f2 power law slope, indicating a random walk.